The International Journal of Engineering and Science (IJES)
|| Volume || 15 || Issue 8 || August || Pages || PP 38-45 || 2026 ||
ISSN (e): 2319 – 1813 ISSN (p): 2319 – 1805

Design And Performance Analysis of Perovskite-Based Solar Cells for High-Efficiency Energy Conversion

DR.Sunil prasad
Assistant professor, PG Department of physics
Rajendra college, chapra.

----------ABSTRACT----------
There is a great deal of room for PSCs to dominate the PV industry since they consume 103 times less resources and have fewer, simpler solution processes than the expensive, high-temperature methods. Solar cells have been the subject of several ongoing studies with the aim of improving their design and functionality. The double PALs, i.e., $MASnI_3$ and $CsSnGeI_3$, are used for simulating the perovskite solar cell utilizing the SCAPS-1D simulating software. Initially, the investigation includes the combined effect of the PAL thicknesses for finding suitable widths for attaining much-improved efficiency of the PSC. In addition, the IDD analysis of the double-graded PSC demonstrates that the state with no interface defect density is the one that may provide the maximum value of output. In addition to that, the QE and JV analysis is also carried out between the single and double PAL in the PSC devices that have been constructed. In comparison to earlier findings by Raghvendra et al. for the lead-free PAL, the current study is a graded technique that is innovative and produces better levels of efficiency.
Keywords- *Performance, Chalcogenides, Spontaneous emission, Photovoltaic cells, Perovskites, power conversion.*

I. INTRODUCTION

Due to its abundance in nature, relative simplicity of circuitry, and relative accessibility of access, solar energy has garnered the most attention among renewable energy supplies. There have been three iterations of solar cells since the first crystalline silicon cells came into being.

Photovoltaic characteristic of perovskite material

Nevertheless, the conversion efficiency still hasn't hit the mark, even when trying out various designs and materials. The very precise photovoltaic characteristic of perovskite material has recently piqued the curiosity of academics. It is a powerful absorber material due to its high absorption coefficient (103 cm^{-1}), charge carrier lifespan, carrier mobility, tuneable band gap, and diffusion length. Shortly after its inception, perovskite solar cells (PSCs) surpassed polycrystalline silicon, the industry leader in photovoltaic (PV) efficiency, and reached solar-to-electric power conversion efficiencies (PCEs) of 25%. [1]

There is a great deal of room for PSCs to dominate the PV industry since they consume 103 times less resources and have fewer, simpler solution processes than the expensive, high-temperature methods. Solar cells have been the subject of several ongoing studies with the aim of improving their design and functionality. A greater band gap allows a perovskite material to absorb photons of higher energy. According to this theory, CZTSe, a chalcogenide material of the second generation, has a smaller band gap and can absorb photons of lower energy. The absorption coefficient of photons by the CZTSe, which can be adjusted to 1 eV, is 105 cm^{-1}.

Perovskite Solar Cells: A New Paradigm in High-Performance Photovoltaic Devices

Because of their dramatically improved Power Conversion Efficiency (PCE), perovskite solar cells (PSCs) have emerged as a promising new alternative to traditional solar cells. After created the first perovskite solar cell in 2009, with an inefficient efficiency of 3.8%, researchers began investigating the material. It something really extraordinary by replacing liquid HTM with solid HTL.[2] This substitution not only solved the issues of recombination and stability, but it also yielded an impressively high efficiency of 9.7 percent. In addition, a meso-superstructure lead-based perovskite solar cell and it had a 10.9% efficiency with very few losses. Snaith et al. developed a compact TiO2 coating for a planar perovskite solar cell later in 2013 using the vapour deposition process; the cell achieved an efficiency of 15.4%. Their efficiency was surpassed by almost 25% in the subsequent nine years. With a band width of 1.5 eV, perovskite solar cells are relatively cheap, have better manufacturability, a high-power conversion efficiency (PCE), and a high absorption coefficient. However, their effectiveness is overshadowed by non-radiative recombination, environmental degradation, and other losses[3].

To successfully reduce non-radiative recombination, current leakage, and other losses, PSCs primarily consist of an absorbing layer, an ETL, and an HTL. Materials with a wider band width are required for photon

trapping. Extraction of electrons from the absorber/active layer and blockage of holes are two of the primary functions of electron transport layers (ETLs) in perovskite solar cells.

There are many common ETLs, including Titanium Dioxide (TiO2), CdZnS, PCBM, and Zinc Oxide (ZnO). With its wide bandgap and excellent chemical stability, TiO2 is thought to be a preeminent ETL material. The typical chemical formula of perovskite crystals is ABX3, where A is the size of a positively charged ion, B is the size of a positively charged ion, and X is the charge of oxygen or halogen ions. Perovskites include positive ions A and B, with A sandwiched between two BX6 octahedrons connected at the apex and B surrounded by negative ions in an octahedron structure; the latter two ions enjoy six-fold coordination. An important part of a solar cell that controls the cell's performance is its active/absorber layer. Due to its role in high charge carrier production and collection, lead-free perovskite improves the performance of the active/absorber layer. Thanks to its remarkable opto-electronic features, such as an adjustable bandgap, extended carrier lifetime, and high light absorption coefficient, the lead-free, non-toxic perovskite material $CH_3NH_3SnI_3$ is used as an active/absorber layer. Like the electron transport layer (ETL) and the absorber layer, the hole transport layer (HTL) is crucial because it blocks electrons while letting holes through. There are a number of popular HTLs that are used, including CuI, NiOx, CuO, CuSCN, Spiro-OMeTAD, P_3HT, PEDOT: PSS, and PTAA.[4]

OBJECTIVE

1. To study on Photovoltaic characteristic of perovskite material
2. To study on Perovskite Solar Cells new Paradigm in High-Performance Photovoltaic Devices

II. METHODOLOGY

Materials and Simulative Inputs

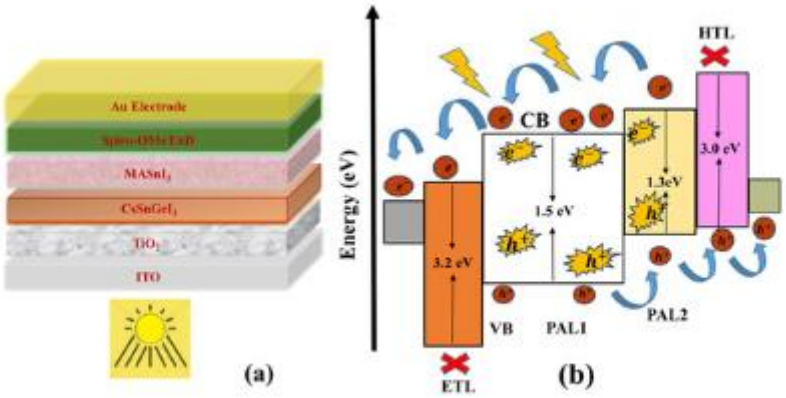

Figure 1. (a) Illustration of PSC device structures; (b) the working mechanism of the PSC at the AM1.5 illuminance.

Figure 1a shows the simulated PSC with an n-i-p arrangement, which corresponds to the three separate layers in the traditional PSC structural design. An electron transport layer (ETL) and a hole transport layer (HTL) are sandwiched around the double absorbing layer (AL). Mesium tin germanium iodide ($CsSnGeI_3$) and methylammonium tin tri-iodide ($MASnI_3$) are the building blocks of the current work's PAL. High efficiency is achieved by confirming the ETL of TiO_2 and the HTL of Spiro-OMeTAD with better outcomes of prior literature findings. There are two reasons why the application of TiO_2 is clear. Two advantages over other ETLs, such MoO_3 and WO_3, are the high carrier mobility and the appropriate band alignment with the PAL. The TiO_2 ETL has a uniform layer with a fine grain structure, which increases the under-layer's surface area and the PSC device's overall efficiency. Furthermore, when compared with other ETL layers, TiO_2 provides superior performance.

Figure 1b shows the process by which the PSC device (CsSnGeI3/MASnI3) operates. In SCAPS-1D, the absorption coefficient α is shown using the formula $\alpha = A\alpha (h\nu - Eg)1/2$, where Eg represents the material's bandgap at the same time. Table 1 contains the input parameters used in this simulation, whereas Table 2 lists the interface defect density (IDD) values. All of the models are run under 100 mW/cm^2 integrated power AM1.5 photo illumination.

Table 1. The input parameters and material characteristics in $CsSnGeI_3$/$MASnI_3$-based PSCs

Parameters	Terms	TiO_2	$MASnI_3$	$CsSnGeI_3$	Spiro-OMeTAD
t (nm)	Thickness	100	200	800	100
Eg (eV)	Bandgap	3.2	1.3	1.5	3.0
χ (eV)	Electron affinity	3.9	4.1	3.9	2.45

εr	Relative permittivity	9	8.2	28	3.0
Nc (cm^{-3})	Effective DoS at CB	1×10^{21}	1×10^{18}	3.1×10^{18}	1×10^{19}
Nv (cm^{-3})	Effective DoS at VB	2×10^{20}	1×10^{18}	3.1×10^{18}	1×10^{19}
μn ($cm^2/V{\cdot}s$)	Electron mobility	20	1.6	974	2×10^{-4}
μp ($cm^2/V{\cdot}s$)	Hole mobility	10	1.6	213	2×10^{-4}
Nd (cm^{-3})	Donor density	1×10^{19}	0	1×10^{14}	0
Na (cm^{-3})	Acceptor density	1	1×10^{15}	0	2×10^{18}
Nt (cm^{-3})	Total defect density	1×10^{14} (donor type)	1×10^{14} (acceptor type)	1×10^{14} (acceptor type)	1×10^{14} (acceptor type)

Table 2. The interface simulation parameters in $MASnI_3$-based PSC device.

Parameters	Spiro-OMeTAD / $MASnI_3$	$MASnI_3$ / $CsSnGeI_3$	$CsSnGeI_3$ / ZnO
Defect types	Neutral	Neutral	Neutral
Capture cross-section (e) (cm^2)	1×10^{-12}	1×10^{-12}	1×10^{-12}
Capture cross-section (h) (cm^2)	1×10^{-12}	1×10^{-12}	1×10^{-12}
Energy distributions	Single	Single	Single
Reference for defect energy level	At Ei	At Ei	At Ei
Total defect density (integrated over all energies) (cm^{-2})	Variable	Variable	Variable

Mathematical Methods

Burgelman et al. found a numerical simulator called SCAPS-1D (Solar Cell Capacitance Simulator) that can reach the significant parameter that determines the outputs of PSCs. To be more precise, under steady-state conditions, the 1D-equation controls the semiconductor materials. Here is one possible representation of the p-n junction electric field-density correlation:[5]

$$\frac{\partial^2 \varphi}{\partial^2 x} = -\frac{\partial E}{\partial x} = -\frac{\rho}{\varepsilon_s} = -\frac{q}{\varepsilon_s}\left[p - n + N_D^+(x) - N_A^-(x) \pm N_{\text{def}}(x)\right]$$

……..(e. q. 1)

The potential difference between two charged particles is seen here as φ; the charge is represented as q; and the static relative permittivity of the medium is depicted by εs. The electrons and the hole are shown as n and p, respectively, while the density of the donor and acceptor is represented as $N^{D}{}_{+}$ and $N^{A}{}_{+}$ Both the donor and the acceptor's defect density are represented by $N_{def}(x)$.

It is also possible to describe the PSC's carrier continuity equation as shown below:

$$-\frac{\partial j_p}{\partial x} + G - U_p(n,p) = 0$$

…….(e. q. 2)

$$\frac{\partial j_n}{\partial x} + G - U_n(n,p) = 0$$

……..(e. q. 3)

The densities of electron and hole currents are j_n and j_p; The rate of carrier production is shown by G; and the rate of recombination for the electron and hole are $U_n(n,p)$ and $U_p(n,p)$, respectively.

At the same time, we may get the carrier current density using the following formula:

$$j_p = qn\mu_p E - qD_p\frac{\partial p}{\partial x}$$

……..(e. q. 4)

$$j_n = qn\mu_n E + qD_n\frac{\partial n}{\partial x}$$

……..(e. q. 5)

where the charge is presented as q and The mobilities of the carriers are shown as μ_p and μ_n while the carriers' diffusion coefficients are D_p and D_n. It should be noted that all the basic perovskite solar cell equations—current density, generation, and rate of recombination—are extracted by the program SCAPS-1D (version 3.8). Finally, a previous paper provides information on how the SCAPS-1D optimizes the recombination losses associated to defects by using some other basic equations.

III. RESULTS AND DISCUSSION

There are five parts to the Results and Discussion section, and they compare and contrast PSCs that use single or dual PALs, as well as the effects of PAL thickness, temperature, and mass defect density. The results may be seen in Figures 2, 3, 4, and 5.

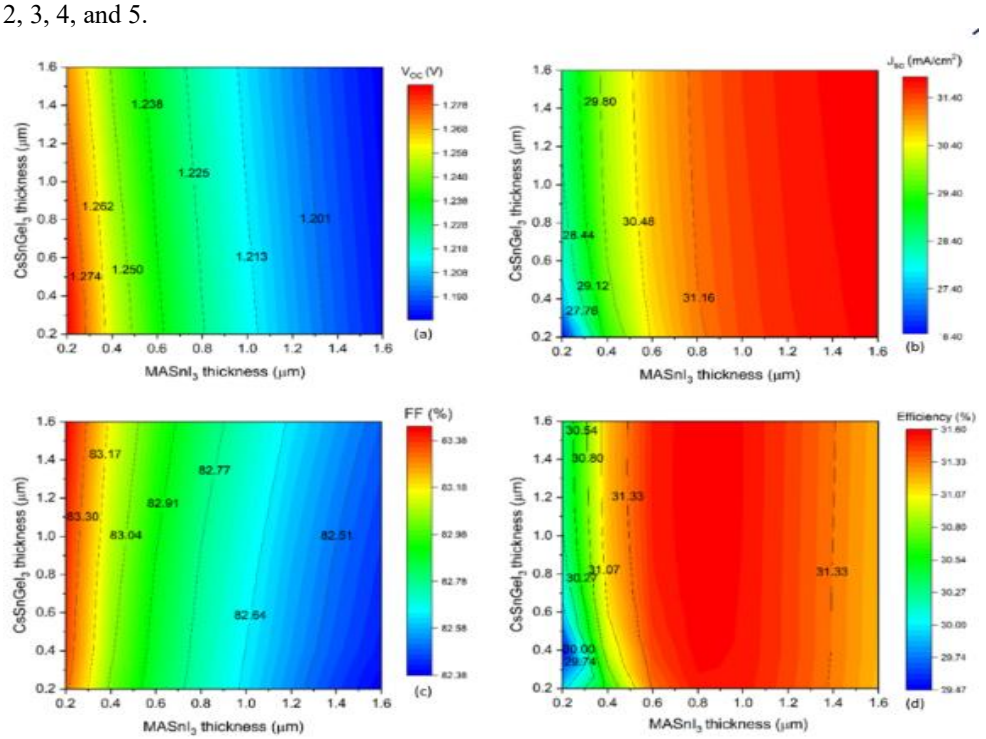

Figure 2. Contour plot of electrical parameters, namely ((a) V_{OC} (V), (b) J_{SC} (mA/cm^2), (c) FF (%) and (d) efficiency (%)) over the PAL thickness of the PSC.

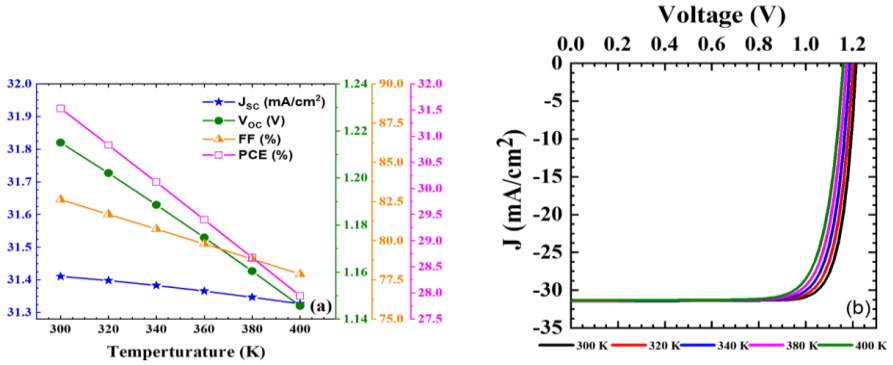

Figure 3. (a) The influence of temperature on solar cell parameters and (b) *J-V* characteristics of the double PAL-based PSC.

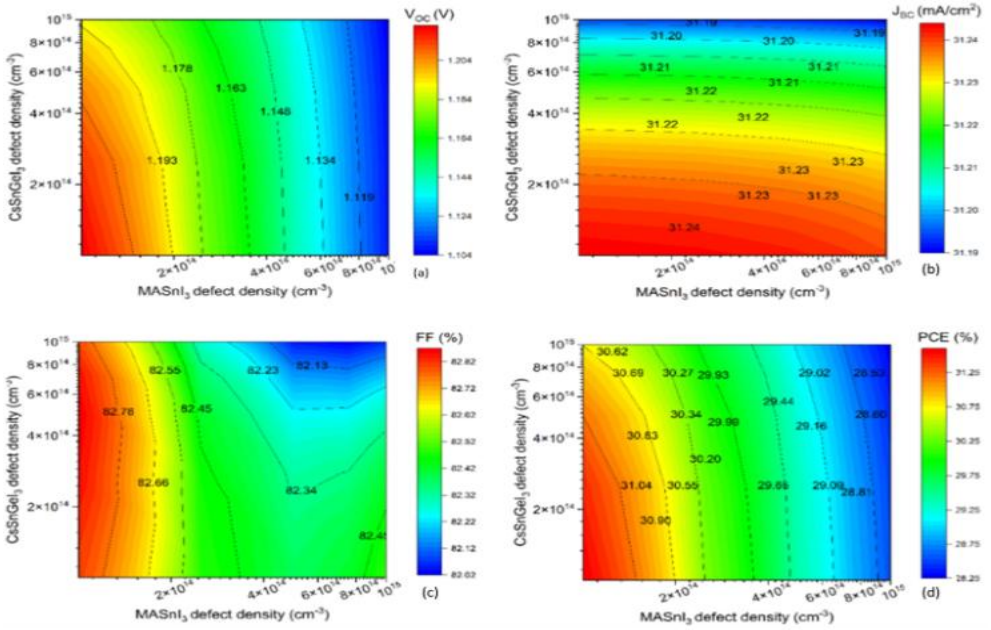

Figure 4. The contour plot of electrical characteristics of (a) *Voc* (V), (b) *Jsc* (mA/cm^2), (c) FF (%) and (d) PCE (%) with the simultaneous arrangement of total DD of the MASnI$_3$/ CsSnGeI$_3$ layer.

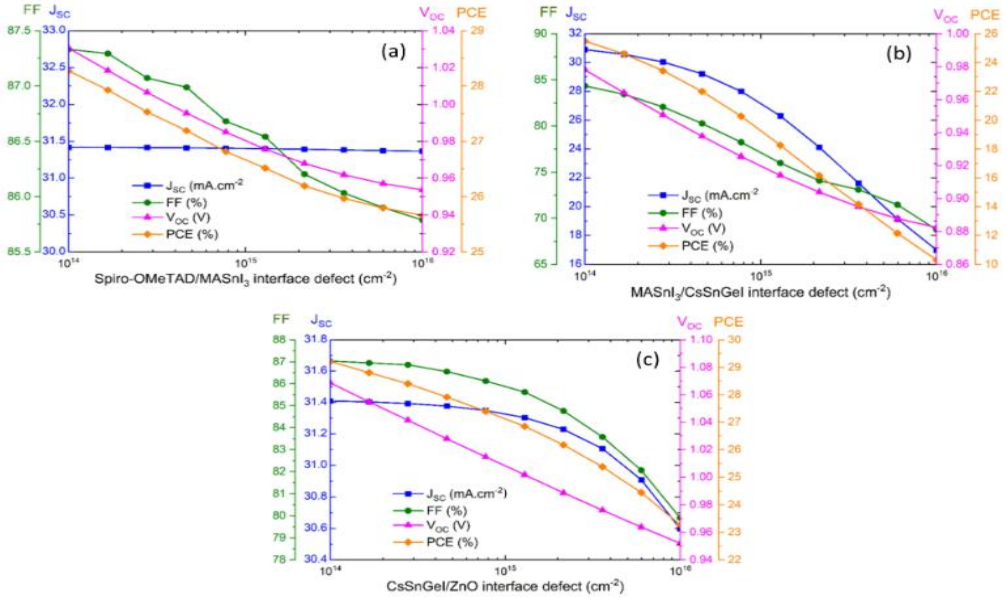

Figure 5. The impact of IDD on the outputs of the PSC; (a) Spiro-OMeTAD/MASnI$_3$, (b) MASnI$_3$/CsSnGeI$_3$ and (c) CsSnGeI$_3$/ZnO, respectively.

Effect of the Combined Thickness of the PALs in PSC

A proportionate analysis of the different thicknesses conducted for the CsSnGeI$_3$- and MASnI$_3$-the active layers are shown on the x- and y-axes. An alternative, more creative method of checking compatibility with thickness is contour plotting, as shown in Figure 2a-d. In order to determine the PSC's optoelectronic properties while exposed to AM1.5 light irradiation, the PV parameters are studied. It can be observed that the V_{OC} is highest for PAL combinations with thinner profiles, providing a value of 1.27 V. For larger conceivable recombination values, the value drops as thickness increases. As far as the J_{SC} is concerned, the MASnI$_3$ thickness of 1.6 µm and 0.2 µm provides a better J_{SC} value offering up to 31.84 mA/cm^2. A minimal value is obtained for a smaller thickness combination of CsSnGeI$_3$ and MASnI$_3$ layers due to inability of photon absorption inside the PALs, obtaining a value of 26.40 mA/cm^2, which further contributes to attaining a smaller efficiency value. In Figure 2c, the dual PAL offers the highest FF of 83.44% at a smaller value of the thicknesses. At last, the effect of the combined thickness over the efficiency is depicted in Figure 2d, as the highest value of efficiency is 31.53% at the thickness of 1 µm and 0.2 µm of MASnI$_3$ and CsSnGeI3, respectively. This is due to the high value of J_{SC} at

the 1 μm level of thickness, since the efficiency is directly related to the PSC's efficiency. Additional characteristics of the PSC device may be simulated using the efficiency range provided by the contour research.

Impact of Temperature on PSC

A thorough comparison of the solar cell properties is used to study the influence of temperature. In Figure 3, we can see how the J_{sc}, V_{oc}, FF, and PCE are affected by temperature. Since the JSC is clearly temperature dependent, it has been steadily declining from 31.41 mA/cm^2 at 300 K to 31.32 mA/cm^2, the V_{oc} also reduces from 1.215 V to 1.18 V; In contrast, the FF value falls as the range of 82.5% to 77.5% increases. Finally, as seen in Figure 3a, the efficiency value provides the maximum efficiency value ranging from 31.53% to 27.9%. Furthermore, the improved PSC shows a more pronounced temperature gradient with an average efficiency of -0.0265%/K.

When studying how temperature affects material characteristics, the SCAPS-1D simulator only solves the three separate equations. In consideration of Equations (6) and (7), the density of states in the valence/conduction band [$N_v(T)/N_c(T)$] fluctuates with the temperature. The thermal velocity $V_{th}(T)$ as seen in Equation (8), is likewise affected by temperature, but the other critical parameters should stay constant, irrespective of changes in temperature. Because it depends on temperature, the diffusion coefficient may be expressed as D = μkT/q. Lastly, the default temperature, T_0, should be specified at 300 K, which is the temperature set in the SCAPS-1D.

$$N_C(T) = N_C(T_0)\left(\frac{T}{T_0}\right)^{1.5} \quad \text{……..(e. q. 6)}$$

$$N_V(T) = N_V(T_0)\left(\frac{T}{T_0}\right)^{1.5} \quad \text{……..(e. q. 7)}$$

$$V_{th}(T) = V_{th}(T_0)\left(\frac{T}{T_0}\right)^{1.5} \quad \text{……..(e. q. 8)}$$

When the temperature rises, all three of the other parameters also rise, including $N_C(T)$, $N_V(T)$ and $V_{th}(T)$, along with the performance that has been noticed. As the density of states rises, electrons and holes have more potential states to conquer. The temperature-dependent thermal velocity affects the material carriers' diffusion, which in turn affects the performance of solar cells. As the temperature rises, the thermal velocity also rises (Equation (8), which means that the carrier lifetime may decrease and the recombination rate might go up. As seen in Figure 3 a, b, this further increases the reverse saturation current and decreases the device performance, especially with regard to V_{oc} and FF. Since the open-circuit voltage drops as the temperature rises due to the temperature dependency of I0, the total V_{oc} drops linearly with the temperature. The temperature gradient described in this study is less than the one in the prior research by Sobayel et al. [6]

Additionally, the J-V characteristics at different temperatures are shown in Figure 3b, which provides accurate information about the effect of temperature. You can get the maximum parameters for the optimal temperature conditions in Table 3. Previous research by Raghhavendra et al. is used to compare PV parameters. to improve efficiency, an absorber based on $CsSnGeI_3$ is used. Since the efficiency drops to 13.29% when using the greater bandgap material in the PSC, the single PAL of broader bandgap perovskite material made of $CsSnGeI_3$ is used instead. Also in Table 3, we can see that Singh et al. achieved an efficiency of up to 20.58% with their single PAL materials, which included a comprehensive optimization method.[7] On the other hand, Noel et al. achieved an efficiency of up to 6.4% with the $MASnI_3$ layer in the PSC.[8]

Table 3. The comparison of solar cell parameters on different device structures.

Device Architectures	VOC (V)	JSC (mA/cm²)	FF (%)	Efficiency (%)
TiO_2 / $CsSnGeI_3$ / Spiro-OMeTAD	1.33	28.27	84.27	28.53
TiO_2 / $MASnI_3$ / $CsSnGeI_3$ / Spiro-OMeTAD	1.215	31.41	82.62	31.53
$CsSnGeI_3$	0.797	20.43	81.63	13.29
$CsSnGeI_3$	1.00	25.75	79.22	20.58
$MASnI_3$	0.88	16.8	42	6.4

Influence of the Total Defect Density (DD) of the Optimized PSC Devices

In Figure 4, we can see how the J_{sc}, V_{oc}, FF, and efficiency PSC outputs are affected by the combined impact of the MASnI3 and $CsSnGeI_3$ layer DD. Under the varying DD range of the $MASnI_3$ and $CsSnGeI_3$ layers, the present study is run using a simulation.1.0×10^{14} cm^{-3} to 1.0×10^{15} cm^{-3}, respectively. The simulation results are attaining the best PSC parameters with JSC of 31.41 mA/cm^2, VOC of 1.215 V, FF of nearly 82.62% and the highest efficiency of 31.53%, at the combined DD of 1.0×10^{14} cm^{-3} because the photo-absorption efficiency of

the $MASnI_3$/$CsSnGeI_3$ active material was optimized. In order to get a more efficient PSC device with double PAL, the combined defect density analysis gives adequate information about the PSC.[9]

EQE and J-V Parameters Comparison of the Simulated PSC Devices

Since the double PAL of $CsSnGeI_3$/$MASnI_3$ absorbs a greater value of wavelengths for the combined low and high bandgaps, it has a slightly lower QE than the single PAL of $CsSnGeI_3$. Only photons with energies greater than the bandgap of the one PAL of $CsSnGeI_3$ are absorbed. So, the single PAL isn't enough to absorb the lower-energy photons. When using double PAL, the photons that pass through the first layer are likewise absorbed by the second layer. As a result, the value of the offering is up to 85% higher than what Azri et al. found before.[10]

The J-V parameter for the improved preconditions for both the single PAL ($CsSnGeI_3$)- and double PAL ($CsSnGeI_3$/$MASnI_3$)-based PSC devices. According to the J-V curve, the JSC value is lower for the single PAL simulation compared to the double PAL simulation. The perovskite material's increased excitons production is a result of its wider photon absorption range. When weighed against, the dual PAL offers a J_{sc} of 31.41 mA/cm^2 while the single PAL offers JSC of 28.27 mA/cm^2, respectively. In contrast, a single PAL in a $CsSnGeI_3$/$MASnI_3$ PSC result in a V_{oc} of 1.33 V, but a double PAL in the same configuration provides a V_{oc} of 1.215 V, a lesser figure that is likely the result of increased recombination within the dual PAL. As shown in Table 3, the results of the improved PSC simulations are reported[11-14].

Influence of IDD on the Output of the PSC

Findings detailed in different parts All the heterojunctions, from A to D, were assumed to have a perfect interface; interfacial recombinations and IDD were not taken into account. Since IDD may significantly affect the solar cell's performance, studying its influence on the PSC is crucial. The PSC's efficiency may be diminished due to the recombination of charge carriers caused by these flaws. Scientists can increase the PSC's effectiveness and reduce the occurrence of IDD by gaining a better grasp of the correlation between the two. Researching how IDD affects perovskite solar cells may provide light on their fundamental physics, which in turn can enhance both the materials and manufacturing methods used to make these cells. Additional simulations are done to obtain the effect of Spiro-OMeTAD/$MASnI_3$ (Figure 5a), $MASnI_3$/$CsSnGeI_3$(Figure 5b) and $CsSnGeI_3$/ZnO (Figure 5c) IDD on the PV performance of the PSC. IDD is varied from 1×10^{14} cm^{-3} to 1×10^{16} cm^{-2}, and corresponding PV parameters are obtained. Spiro-OMeTAD/$MASnI_3$ IDD variation showed negligible effect on JSC but significantly reduced the V_{oc} from 1.03 V to 0.95 V while it increased the IDD from 1×10^{14}cm^{-2} to 1×10^{16} cm^{-2}. FF was also reduced from 87.3% to 85.8%. IDD can create recombination centers that reduce the efficiency of charge transport in the cell, which can lead to a decrease in the VOC and FF. The collective effect of JSC, VOC and FF led to a reduction in overall PCE from 28.3% to 25.7%. A similar trend is also observed for $MASnI_3$/$CsSnGeI_3$ and $CsSnGeI_3$/ZnO IDD, which showed a reduction in PCE from 25.5% to 10.3% and 29.2% to 23.3% while an increase in IDD from 1×10^{14} cm^{-2} to 1×10^{16} cm^{-2}, respectively. Further, detailed PV parameters are also tabulated in Table 4 with each combination of three different cases, i.e., No IDD, IDD at 1×10^{14} cm^{-2}, and IDD at 1×10^{16}cm^{-2} for all three interfaces. Results showed that the $MASnI_3$/$CsSnGeI_3$ interface greatly impacted the PV performance compared to the other two interfaces. Also, Table 4 describes the detailed comparison of the IDD values of all three interfaces. From no DD to 1×10^{16} cm^{-2}, the variation is recorded to obtain the best combination of the IDD levels[15-17].

IV. CONCLUSIONS

The double PALs, i.e., $MASnI_3$ and $CsSnGeI_3$, are used for simulating the perovskite solar cell utilizing the SCAPS-1D simulating software. Initially, the investigation includes the combined effect of the PAL thicknesses for finding suitable widths for attaining much-improved efficiency of the PSC. It can be depicted that the output parameters of the PSC are considerably enhanced by utilizing the thickness of 1 µm and 0.2 µm, respectively. The next evident outcome of the current work is that the defect density of both the PALs is the lowest value of defect density, i.e., 1.0×10^{14} cm^{-3}, which offers an improvement in the efficiency of up to 31.53%. The investigation of the influence of the temperature also illustrates that the 300 K temperature can be suitable for the effective production of the PSC, and an increment in the temperature further impacts the V_{oc} the present research deserves recognition since it is a good example of how the effective combination of suitable CTLs may enhance efficiency and get it closer to the Shockley-Queisser limit. In addition, the IDD analysis of the double-graded PSC demonstrates that the state with no interface defect density is the one that may provide the maximum value of output. In addition to that, the QE and JV analysis is also carried out between the single and double PAL in the PSC devices that have been constructed. In comparison to earlier findings by Raghvendra et al. for the lead-free PAL, the current study is a graded technique that is innovative and produces better levels of efficiency. As well as being vital for the non-toxicity of the materials that are being created, the outcome of the current simulation is also significant. Therefore, the present work offers a superior alternative for attaining cost-effective and higher device productivity for PSC devices that have been created correctly.

REFERENCES

[1.] H. Zhou, Q. Chen, G. Li, S. Luo, T. Song, H. Duan, Z. Hong, J. You, Y. Liu, and Y. Yang, "Interface engineering of highly efficient perovskite solar cells," Science, vol. 345, no. 6196, p. 542 - 546, Aug. 2014.

[2.] Y. Wu, F. Xie, H. Chen, 11, no. 1, p. 2878, Jun. 2020.

[3.] Snaith, H.J. Perovskites: The Emergence of a New Era for Low-Cost, High-Efficiency Solar Cells. J.Phys. Chem. Lett. 2013, 4, 3623–3630.

[4.] Ahmed, M.I.; Habib, A.; Javaid, S.S. Perovskite Solar Cells: Potentials, Challenges, and Opportunities. Int. J. Photoenergy 2015, 2015, 592308. [Google Scholar] [CrossRef]

[5.] Burgelman, M.; Verschraegen, J.; Degrave, S.; Nollet, P. Modeling Thin-Film PV Devices. Prog. Photovoltaic. Res. Appl. 2004, 12, 143–153.

[6.] Sobayel, K.; Rahman, K.S.; Karim, M.R.; Aijaz, M.O.; Dar, M.A.; Shar, M.A.; Misran, H.; Amin, N. Numerical Modeling on Prospective Buffer Layers for Tungsten Di-Sulfide (WS2) Solar Cells by Scaps-1D. *Chalcogenide Lett.* **2018**, *15*, 307–315.

[7.] Kojima, A.; Teshima, K.; Shirai, Y.; Miyasaka, T. Raghhavendra , Organometal Halide Perovskites as Visible-Light Sensitizers for Photovoltaic Cells. J.Am. Chem. Soc. 2009, 131, 6050–6051.

[8.] Noel, N.K.; Stranks, S.D.; Abate, A.; Wehrenfennig, C.; Guarnera, S.; Haghighirad, A.A.; Sadhanala, A.; Eperon, G.E.; Pathak, S.K.; Johnston, M.B.; et al. Lead-Free Organic-Inorganic Tin Halide Perovskites for Photovoltaic Applications. *Energy Environ. Sci.* **2014**, *7*, 3061–3068..

[9.] Lakhdar, N.; Hima, A. Electron Transport Material Effect on Performance of Perovskite Solar Cells Based on CH3NH3GeI3. Opt. Mater. 2020, 99, 109517.

[10.] Karthick, S.; Velumani, S.; Bouclé, J. Experimental and SCAPS Simulated Formamidinium Perovskite Solar Cells: A Comparison of Device Performance. Sol. Energy 2020, 205, 349–357.

[11.] Raoui, Y.; Ez-Zahraouy, H.; Tahiri, N.; El Bounagui, O.; Ahmed, S.; Kazim, S. Performance Analysis of MAPbI3 Based Perovskite Solar Cells Employing Diverse Charge Selective Contacts: Simulation Study. Sol. Energy 2019, 193, 948–955.

[12.] Bhattarai, S.; Das, T.D. Optimization of the Perovskite Solar Cell Design to Achieve a Highly Improved Efficiency. Opt. Mater. 2021, 111, 110661.

[13.] Singh, N.; Agarwal, A.; Agarwal, M. Numerical Simulation of Highly Efficient Lead-Free Perovskite Layers for the Application of All-Perovskite Multi-Junction Solar Cell. Superlattices Microstructure. 2021, 149, 106750.

[14.] Nalianya, M.A.; Awino, C.; Barasa, H.; Odari, V.; Gaitho, F.; Omogo, B.; Mageto, M. Numerical Study of Lead Free CsSn0.5Ge0.5I3 Perovskite Solar Cell by SCAPS-1D. Optik 2021, 248, 168060.

[15.] Kumari, K.; Jana, A.; Dey, A.; Chakrabarti, T.; Sarkar, S.K. Lead Free CH3NH3SnI3 Based Perovskite Solar Cell Using ZnTe Nano Flowers as Hole Transport Layer. Opt. Mater. 2021, 111, 110574.

[16.] Singh, A.K.; Srivastava, S.; Mahapatra, A.; Baral, J.K.; Pradhan, B. Performance Optimization of Lead Free-MASnI3 Based Solar Cell with 27% Efficiency by Numerical Simulation. Opt. Mater. 2021, 117, 111193.

[17.] Raghavendra; Kumar, R.R.; Pandey, S.K. Performance Evaluation and Material Parameter Perspective of Eco-Friendly Highly Efficient CsSnGeI3 Perovskite Solar Cell. Superlattices Microstructure. 2019, 135, 106273.